Quasi first-order Hermite Gaussian beam for enhanced sensitivity in Sagnac interferometer photothermal deflection spectroscopy

Naoyuki Shiokawa and Eiji Tokunaga*

Department of Physics, Faculty of Science, Tokyo University of Science, 1-3 Kagurazaka, Shinjuku-ku, Tokyo 162-8601, Japan

eiji@rs.kagu.tus.ac.jp

Abstract: The detection sensitivity of a Sagnac interferometer photothermal deflection spectroscopy was enhanced by changing the probe beam pattern from zero-order to a quasi-first-order Hermite Gaussian (QHG) beam. The nature of the higher order HG mode, where the beam pattern is preserved during propagation with an increased field gradient, is utilized to enhance the measurement sensitivity. In this spectroscopy, the lateral beam deflection due to the photothermal effect is sensitively detected as a change in the interference light intensity. The change in intensity is amplified due to the higher field gradient of the QHG(1,0) beam at the photodetector. This amplification effect was both numerically and experimentally demonstrated to obtain twofold improvement in the signal-to-noise ratio.

OCIS codes: (300.6430) Spectroscopy, photothermal; (120.3180) Interferometry; (120.5790) Sagnac effect; (140.3300) Laser beam shaping; (190.4870) Photothermal effects.

References and links

1. W. B. Jackson, N. M. Amer, A. C. Boccara, and D. Fournier, "Photothermal deflection spectroscopy and detection," Appl. Opt. **20**(8), 1333–1344 (1981).
2. O. O. Dada and S. E. Bialkowski, "A Compact, Pulsed Infrared Laser-Excited Photothermal Deflection Spectrometer," Appl. Spectrosc. **65**(2), 201–205 (2011).
3. N. G. C. Astrath, L. C. Malacame, G. V. B. Lukaseivicz, H. S. Bernabe, J. H. Rohling, M. L. Baesso, J. Shen, and S. E. Bialkowski, "A 3-dimensional time-resolved photothermal deflection "Mirage" method," Appl. Phys. Lett. **100**(9), 091908 (2012).
4. E. Buchaca-Domingo, K. Vandewal, Z. Fei, S. E. Watkins, F. H. Scholes, J. H. Bannock, J. C. de Mello, L. J. Richter, D. M. DeLongchamp, A. Amassian, M. Heeney, A. Salleo, and N. Stingelin, "Direct Correlation of Charge Transfer Absorption with Molecular Donor:Acceptor Interfacial Area via Photothermal Deflection Spectroscopy," J. Am. Chem. Soc. **137**(16), 5256–5259 (2015).
5. M. Yorulmaz, S. Nizzero, A. Hoggard, L. Y. Wang, Y. Y. Cai, M. N. Su, W. S. Chang, and S. Link, "Single-Particle Absorption Spectroscopy by Photothermal Contrast," Nano Lett. **15**(5), 3041–3047 (2015).
6. S. Ilahi, F. Saidi, R. Hamila, N. Yacoubi, L. Auvray, and H. Maaref Curr, "Photothermal deflection spectroscopy (PDS) investigation of optical and thermal properties of BGaAs/GaAs alloys," Appl. Phys. (Berl.) **13**(3), 610–613 (2013).
7. G. Leahu, R. Li Voti, S. Paoloni, C. Sibilia, and M. Bertolotti, "Trace gas analysis from glazes by means of a compact photothermal deflection spectroscopy apparatus," Rev. Sci. Instrum. **84**(12), 123111 (2013).
8. T. Toyama, Y. Seo, T. Konishi, H. Okamoto, R. Morimoto, Y. Nishikawa, and Y. Tsutsumi, "Optical absorption spectra of P-type Tin monoxide thin films around their indirect fundamental gaps determined using photothermal deflection spectroscopy," Thin Solid Films **555**, 148–152 (2014).
9. A. C. Tam, Rev. "Applications of photoacoustic sensing techniques," Mod. Phys. **58**(2), 381–431 (1986).
10. T. Kitamori and T. Sawada, "Novel Analytical and Chemometric Applications of Photothermal Spectroscopy," Spectrochim. Acta Rev. **14**(4), 275–302 (1991).
11. A. Harata, Q. Shen, and T. Sawada, "Photothermal applications of lasers: study of fast and ultrafast photothermal phenomena at metal-liquid interfaces," Annu. Rev. Phys. Chem. **50**(1), 193–219 (1999).
12. Y. Nosaka and E. Tokunaga, "Development of photoacoustic spectroscopy with a piezofilm," Appl. Opt. **46**(20), 4289–4293 (2007).

#261242 Received 16 Mar 2016; revised 22 Apr 2016; accepted 27 Apr 2016; published 24 May 2016

13. Y. Nosaka and E. Tokunaga, "Development of photoacoustic spectroscopy with a piezofilm: errata," Appl. Opt. **46**(29), 7267 (2007).
14. S. Berciaud, L. Cognet, and B. Lounis, "Photothermal absorption spectroscopy of individual semiconductor nanocrystals," Nano Lett. **5**(11), 2160–2163 (2005).
15. J. He, J. Miyazaki, N. Wang, H. Tsurui, and T. Kobayashi, "Biological imaging with nonlinear photothermal microscopy using a compact supercontinuum fiber laser source," Opt. Express **23**(8), 9762–9771 (2015).
16. N. Shiokawa, Y. Mizuno, H. Tsuchiya, and E. Tokunaga, "Sagnac interferometer for photothermal deflection spectroscopy," Opt. Lett. **37**(13), 2655–2657 (2012).
17. S. Yukita, N. Shiokawa, H. Kanemaru, H. Namiki, T. Kobayashi, and E. Tokunaga, "Deflection switching of a laser beam by the Pockels effect of water," Appl. Phys. Lett. **100**(17), 171108 (2012).
18. T. Takahashi, Y. Ishii, and R. Onodera, "Phase-shifting interferometric profilometry with a wavelength-tunable diode source," Opt. Rev. **21**(3), 410–414 (2014).
19. P. G. Lucey, K. A. Horton, and T. Williams, "Performance of a long-wave infrared hyperspectral imager using a Sagnac interferometer and an uncooled microbolometer array," Appl. Opt. **47**(28), F107–F113 (2008).
20. K. Misawa and T. Kobayashi, "Femtosecond Sagnac interferometer for phase spectroscopy," Opt. Lett. **20**(14), 1550–1552 (1995).
21. D. N. Naik, T. Ezawa, R. K. Singh, Y. Miyamoto, and M. Takeda, "Coherence holography by achromatic 3-D field correlation of generic thermal light with an imaging Sagnac shearing interferometer," Opt. Express **20**(18), 19658–19669 (2012).
22. M. C. Gabriel, N. A. Whitaker, Jr., C. W. Dirk, M. G. Kuzyk, and M. Thakur, "Measurement of ultrafast optical nonlinearities using a modified Sagnac interferometer," Opt. Lett. **16**(17), 1334–1336 (1991).
23. T. Shirai, T. H. Barnes, and T. G. Haskel, "Surface-profile measurement by means of a polarization Sagnac interferometer with parallel optical feedback," Opt. Lett. **24**(5), 297–299 (1999).
24. T. Kim, M. Fiorentino, and F. N. C. Wong, "Phase-stable source of polarization-entangled photons using a polarization Sagnac interferometer," Phys. Rev. A **73**(1), 012316 (2006).
25. S. C. Chu, Y. T. Chen, K. F. Tsai, and K. Otsuka, "Generation of high-order Hermite-Gaussian modes in end-pumped solid-state lasers for square vortex array laser beam generation," Opt. Express **20**(7), 7128–7141 (2012).
26. M. W. Beijersbergen, L. Allen, H. E. L. O. van der Veen, and J. P. Woerdman, "Astigmatic laser mode converters and transfer of orbital angular momentum," Opt. Commun. **96**(1–3), 123–132 (1993).
27. Y. F. Chen, T. M. Huang, C. F. Kao, C. L. Wang, and S. C. Wang, "Generation of Hermite–Gaussian modes in fiber-coupled laser-diode End-pumped lasers," IEEE J. Quantum Electron. **33**(6), 1025–1031 (1997).
28. Y. Yoshikawa and H. Sasada, "Versatile generation of optical vortices based on paraxial mode expansion," J. Opt. Soc. Am. A **19**(10), 2127–2133 (2002).
29. T. Meyrath, F. Schreck, J. Hanssen, C. Chuu, and M. Raizen, "A high frequency optical trap for atoms using Hermite-Gaussian beams," Opt. Express **13**(8), 2843–2851 (2005).

1. Introduction

Photothermal deflection spectroscopy (PDS) [1–8] is one of photothermal conversion spectroscopic methods [9–15] that are widely used to examine the optical properties of materials. In PDS, the photothermal deflection effect is utilized to measure the absorption spectra of samples that exhibit significant scattering, such as powders, or optically thick samples that have no transmission. Heat generated by absorption is detected by PDS as the deflection of a laser beam.

The photothermal deflection effect is illustrated in Fig. 1, where a sample is photoexcited from above and a probe laser is transmitted through the surrounding medium (deflection medium) just above the sample. The temperature distribution formed by heat due to the non-radiative relaxation of the photoexcited sample is converted into a refractive index distribution by the temperature coefficient of the refractive index (dn/dT) in the surrounding deflection medium. The wavefront of the laser beam passing through a high refractive index region travels behind that passing through a low refractive index region, which results in a deflection of the beam as expressed by the deflection angle $\Delta\theta$ in Fig. 1. This is referred to as the photothermal deflection effect.

#261242 Received 16 Mar 2016; revised 22 Apr 2016; accepted 27 Apr 2016; published 24 May 2016

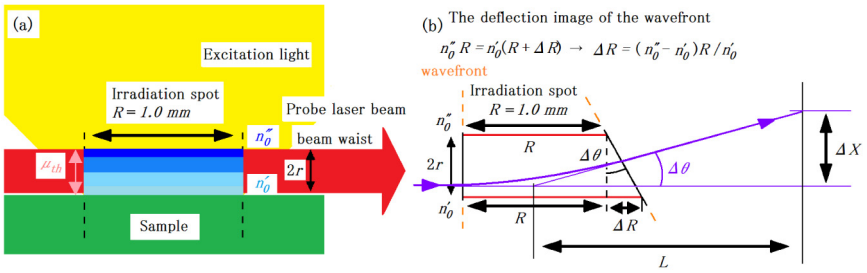

Fig. 1. Schematic diagram of the probe laser beam deflection in the refractive index distribution formed by the excitation light above the sample. This figure shows the spatial arrangement (a) and the detailed description of laser beam deflection (b).

To increase the deflection angle of the laser beam, carbon tetrachloride is often used as a deflection medium because it has a large dn/dT to induce a greater spatial refractive index gradient. The deflection angle of the laser beam is detected as a function of the excitation light wavelength, which indicates the amount of the nonradiative relaxation processes, i.e., a photothermal spectrum of the sample is obtained. This is equivalent to the absorption spectrum under appropriate conditions. In general, the deflection angle is very small, so that a highly sensitive method for measurement of the angle is required in PDS.

In conventional PDS, the laser beam deflection is measured with a position sensitive detector (PSD) as a change in the center position of the laser beam. A tunable laser light source for excitation and carbon tetrachloride (CCl_4) as a deflection medium are generally used to increase the signal intensity, i.e., the deflection angle, at the expense of a wide spectral range and a variety of measurable samples (restricted to materials insoluble in the non-polar solvent). We have previously developed a Sagnac interferometer PDS [16, 17] to achieve a major improvement in the sensitivity of this method. As a result, photothermal spectra were obtained even with a monochromated Xe lamp as the excitation light and with air or water as the deflection medium.

For high sensitivity measurement, many types of interferometers are devised and adapted for various studies such as distance measurement [18] and so on. A Sagnac interferometer is one of the interferometers that have a common-path characteristics where common noise, such as the vibrational noise of the optical system, is suppressed. By utilizing the phase stability, Sagnac interferometers have been applied for imaging techniques [19–21], optical nonlinearity measurements [22], surface shape measurements [23], and the generation of entangled photons [24]. In conventional PDS, the sensitivity cannot be improved by extending the optical path, because not only the signal but also the vibrational noise is amplified in proportion to the optical path length; by contrast, we have successfully amplified only the signal by extending the optical path using a Sagnac interferometer [16]. Two laser beam wavefronts were generated from one wavefront of a laser beam using a beam splitter (BS) where the wavefront enters the Sagnac interferometer. The relative phase of these wavefronts is fixed at π to achieve destructive interference after passing through the interferometer. The interference intensity is continuously changed by changing the degree of overlap of the two laser beam wavefronts. Thus, a change in the position (X) of the probe laser beam is converted into a change in the interference intensity (I) dependent on dI/dX . Therefore, a photodiode (PD) is used as a detector instead of a PSD. This is also one of the reasons the signal to noise ratio (S/N) can be improved, because the dark current is much smaller in a PD than in a PSD.

In this work, the S/N is further improved by the use of a probe laser beam with a high order spatial mode in Sagnac interferometer PDS, where the excitation light is a white-light lamp and the deflection medium is air [16]. There have been a number of basic research reports regarding the generation and spatial propagation characteristics of high order Hermite

#261242 Received 16 Mar 2016; revised 22 Apr 2016; accepted 27 Apr 2016; published 24 May 2016

Gaussian (HG) laser beams [25–28]; however, there are only a few reports on their application, such as a beam trap [29]. In this paper, for the first time to our knowledge, high-order HG modes of a laser beam are successfully applied to improve the sensitivity of signal detection. A zero-order HG beam [HG(0,0)] is typically used as a probe laser beam for Sagnac interferometer PDS. If the probe laser beam mode is converted into a higher order Hermite-Gaussian mode, then the spatial beam pattern is preserved during propagation to increase the slope of the spatial electric field at any position along the path. Thus, dI/dX can be increased at the detector position, whereby the S/N of Sagnac interferometer PDS can be improved.

2. Detection principle of Sagnac PDS

2.1. Physical parameters in PDS

In this section, the principle of the photothermal deflection effect mentioned in the introduction is explained in detail. The heat generated by non-radiative relaxation of the sample is spread only in the vicinity of the sample, so that the probe laser beam is needed to pass through the volume with thermal distribution caused by heat generation. The spreading length of the heat called thermal diffusion length μ_{th} is given by

$$\mu_{\text{th}} = \sqrt{\frac{\kappa}{\rho C_{\text{p}} \pi f}} \tag{1}$$

where ρ is the density, κ is the thermal conductivity, C_{p} is the specific heat at constant pressure, and f is the modulation frequency. Thermal distribution determined by μ_{th} is transformed into the refractive index distribution through the temperature coefficient of the refractive index, which is defined by

$$\frac{dn}{dT} = \frac{(n^2-1)(n^2+2)}{6n} 3\alpha, \tag{2}$$

where α is the coefficient of linear expansion and n is the refractive index. The refractive index distribution deflects the probe laser beam. Figure 1 depicts the deflection of the probe laser beam, which is transmitted through just above the excited spot of a circle with a diameter R. When the refractive index varies from n_0' to n_0'' within the probe beam diameter directly above the excited spot, the difference of the optical path length is given by $(n_0'' - n_0')R$. The laser beam waist $2r$ at the sample position is determined by the focal length of the lens, so that it can be adjusted to the thermal diffusion length μ_{th}. If the difference in the optical path length occurs only in the rectangular $2rR$ region indicated in Fig. 1(b), The wavefront is so determined that the equation for the optical path length, $n_0'' R = n_0'(R + \Delta R)$, holds. Then, the deflection angle $\Delta\theta$ is given by

$$\tan\Delta\theta = \frac{\Delta R}{2r} = \frac{(n_0'' - n_0')R}{2n_0' r}. \tag{3}$$

The refractive index variation Δn and the temperature change ΔT are represented by $\Delta n = n_0'' - n_0'$ and $\Delta T = (dT/dn)\Delta n$, respectively. If the optical path length from the sample position to the detector is L, then the displacement ΔX at the detector position is expressed by $\Delta X = L\tan\Delta\theta$. The temperature change ΔT at the excitation spot is estimated with the known parameters by

#261242 Received 16 Mar 2016; revised 22 Apr 2016; accepted 27 Apr 2016; published 24 May 2016

$$\Delta T = \frac{2n_0' r \Delta X}{LR} \frac{dT}{dn}. \tag{4}$$

In this way, the temperature change ΔT is estimated with the detected deflection.

2.2. Detecting the laser beam deflection with the Sagnac interferometer

In Sagnac PDS, the laser beam deflection is detected as a change in the interference light intensity with displacement. The displacement ΔX is detected by converting it to the change in the interference light intensity using a Sagnac interferometer. The Sagnac interferometer was constructed with one beam splitter (BS) and three mirrors. The probe laser beam is split into the two beams with the BS. For convenience, the two probe laser beams are referred to as the clockwise direction (CW) and counterclockwise direction (CCW), which travel through the common optical path to be superposed and interfere destructively after transmission through the same BS (dark port). Destructive interference occurs because the two laser beams (CW and CCW) have a phase difference of π after being subjected to a different number of fixed end reflections. The Sagnac interferometer used is shown in Fig. 2.

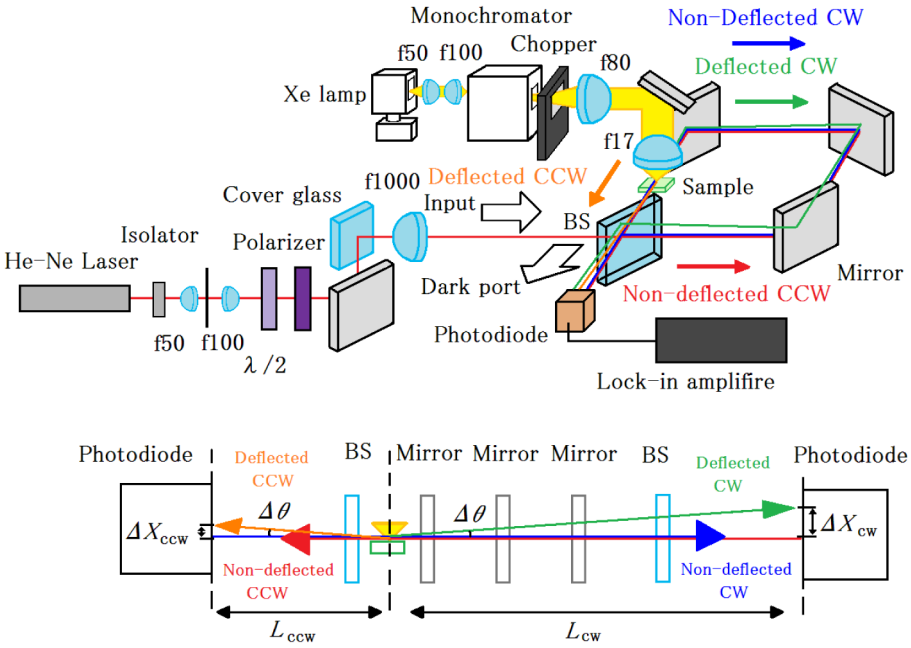

Fig. 2. Sagnac interferometer with one beam splitter (BS) and three mirrors. The input laser beam is divided by the BS into clockwise (CW) and counterclockwise (CCW) beams, which are propagated through a common path to be recombined at the BS and exit at the dark port to produce destructive interference.

The sample is placed in an asymmetrical position in the optical path of the Sagnac interferometer for PDS. If the sample is located at the symmetrical position, then displacement of the CW and CCW laser beams caused by deflection would be canceled, and the change in the light intensity would also be canceled.

When the optical path lengths from the sample position to the detector for CW and CCW are L_{CW} and L_{CCW} respectively, ΔX_{CW} and ΔX_{CCW} for the displacement for CW and CCW are represented by $L_{CW} \tan \Delta\theta$ and $L_{CCW} \tan \Delta\theta$, respectively. In this experiment, the excitation light was irradiated on the sample from above, and the laser beams were propagated through just above the irradiated spot. Thus, the CW and CCW beams deflect upwards. The

#261242 Received 16 Mar 2016; revised 22 Apr 2016; accepted 27 Apr 2016; published 24 May 2016

interference light intensity I at the dark port of the Sagnac interferometer is calculated by integration of the squared amplitude of the spatial electric field formed by CW and CCW. When CW and CCW are the HG(0,0) beams and the initial distance between the center of CW and CCW is X, the integrated interference light intensity (power) $I_{(0,0)}$ is represented by

$$I_{(0,0)} = I_0(1-e^{-\frac{X^2}{2w^2}}) \propto \iint dxdy \left| E_{(0,0)}(x-\frac{X}{2},y) - E_{(0,0)}(x+\frac{X}{2},y) \right|^2, \tag{5}$$

where

$$E_{(0,0)}(x,y) = E_0 e^{-(\frac{x^2+y^2}{w^2})}. \tag{6}$$

$E_{(0,0)}$ is the electric field of the HG(0,0) laser beam and w is the radius of the beams. The coefficient I_0 is a normalization factor for the power of two laser beams after the Sagnac interferometer when the initial distance X is a positive infinite value. Thus, the change in the light intensity with displacement ΔX is represented by

$$\frac{dI_{(0,0)}}{dX} = I_0 \frac{X}{w^2} e^{-\frac{X^2}{2w^2}} = I_0 \frac{Y}{w} e^{-\frac{Y^2}{2}}, \tag{7}$$

where the parameter Y is X/w. Equation (7) describes the change in the interference light intensity with displacement. The $dI_{(0,0)}/dX$ takes the maximum value when the parameter Y is 1.0. These equations are shown in Fig. 3 by using the experimental value w. The maximum value increases if the radius w is decreased. But if the radius w is reduced by focusing with a focusing lens before the detector, the detection sensitivity increases while the displacement ΔX decreases. The signal intensity at the photodiode is given by the sensitivity dI/dX multiplied with the displacement ΔX. Therefore, the increase in the sensitivity is just canceled by the decrease in the displacement. By contrast, the mode conversion can generate a beam that has higher sensitivity dI/dX without use of a focusing lens. Thus the signal intensity at the photodiode increases for the same amount of displacement ΔX.

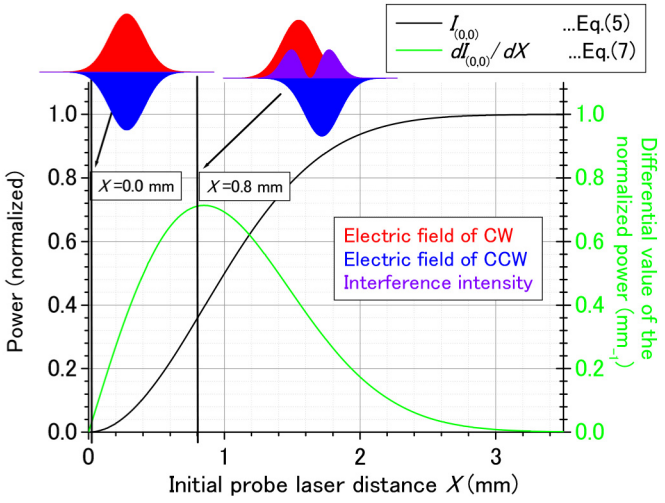

Fig. 3. Power $I_{(0,0)}$ for the HG(0,0) (black line) and the differential of $I_{(0,0)}$ (green line) as a function of X, the lateral displacement between the CW and CCW beams at the dark port of the Sagnac interferometer. The power is normalized with respect to the intensity when the two beams are completely separated.

#261242 Received 16 Mar 2016; revised 22 Apr 2016; accepted 27 Apr 2016; published 24 May 2016

2.3. Conversion of the beam spatial pattern

The standard method to generate a higher order Hermite Gaussian beam is to insert a thin tungsten wire in a laser cavity [26] or to introduce imbalance into a laser cavity [27]; however, this requires manipulation of the laser apparatus itself and does not involve the conversion of propagating beams. Instead, a method to convert propagating HG(0,0) beams to the higher order modes is proposed using tilted glass plates [28]. Following this method, the order of the HG beam was converted to the quasi-HG mode (QHG) using reflection by a cover glass in the present experiment. Figure 4 shows a schematic diagram of the method.

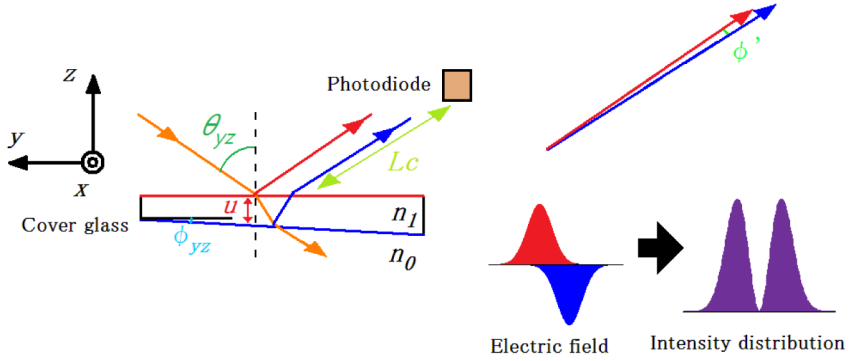

Fig. 4. Schematic diagram of the beam spatial pattern conversion method using a cover glass. The red and blue lines indicate the front and back surfaces of the cover glass. The beams reflected from these surfaces are depicted as red and blue arrows. The red and blue colored Gaussian distributions are the respective electric field images of the laser beams reflected from the front and back surfaces, and the violet colored intensity distribution image is the result of destructive interference of these electric fields.

The front and back surfaces of the cover glass produce two wavefronts from the incident laser beam. The xy plane and z-axis were taken as the front surface of the cover glass and the axis normal to it, respectively. The front and back surfaces were not completely parallel but made a small angle ϕ_{yz} on the cross section of the yz plane, while those on the xz plane were almost parallel, thereby making a negligibly small angle $\Phi_{xz}(<<\Phi_{yz})$. When the laser beam was incident on the front surface with a small incident angle θ_{yz}, the angle ϕ' between the traveling directions of the two reflected beams from the front and back surfaces is $2\phi_{yz}(n_1/n_0)$ if ϕ_{yz} and θ_{yz} are sufficiently small. Here, n_0 and n_1 are the refractive indices of air and the cover glass, respectively. When the distance from the cover glass to the PD is L_c, the separation between the center of two beams that are reflected by the cover glass is $L_c \tan\phi'$ at the PD. Appropriate adjustment of θ_{yz}, ϕ_{yz}, and the cover glass thickness u, enable the phase difference π to be produced between the two reflected beams. Experiments were attempted with three or four cover glasses until the optimum conditions were attained. As a result, the two laser beams interfered destructively to produce an intensity distribution similar to the first order HG mode [HG(1,0)]. However, the propagation characteristics were different from the HG(1,0) mode, so that the beam pattern converted by the cover glass is referred to as a QHG beam [28]. The spatial distribution of the electric field of CW at the PD position of the optical path length L_c from the cover glass is expressed by

$$E = E_0\left(e^{-\frac{(x+\frac{L_c}{2}\tan\phi')^2+y^2}{w^2}} + e^{-\frac{(x-\frac{L_c}{2}\tan\phi')^2+y^2}{w^2}} e^{ik\frac{2n_1u}{\sqrt{1-\frac{n_0}{n_1}\sin\theta_{yz}}}\left(\frac{n_0}{n_1}-1\right)\sin\theta_{yz}}\right), \quad (8)$$

#261242 Received 16 Mar 2016; revised 22 Apr 2016; accepted 27 Apr 2016; published 24 May 2016

where u is the thickness of the cover glass at the reflected position. When appropriate values for θ_{yz}, ϕ', and u were obtained by fine-tuning together with three or four replacements of the cover glass, Eq. (8) is rewritten as

$$E_{(1,0)}(x,y) = E_0(e^{-\frac{(x+\frac{D}{2})^2+y^2}{w^2}} - e^{-\frac{(x-\frac{D}{2})^2+y^2}{w^2}}), \tag{9}$$

which yields a laser beam with a QHG(1,0) transverse mode at the PD, where D is the distance between the centers of the HG(0,0) beams. The beam radius w was 0.85 mm for HG(0,0) in the experiment. The light intensity distribution of the HG(0,0) and QHG(1,0) beam is shown in Fig. 5.

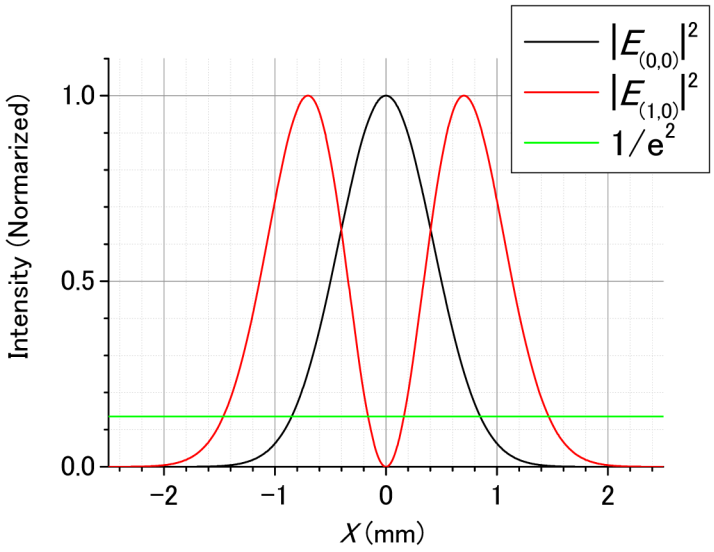

Fig. 5. Light intensity distributions of the HG(0,0) (black line) and QHG(1,0) (red line) beams. The green line indicates the value for $1/e^2$.

The QHG(1,0) mode has a sharp beam pattern compared to the HG(0,0) mode with a larger gradient. The optical path length L_c in the experiment was 2.5 m, whereby ϕ' was determined to be 0.9 mrad from L_c and D.

2.4. Displacement detection with a high order HG beam

The power detected at the PD is given by:

$$I_{(1,0)} = I_0[1 - \frac{1}{(1-e^{-\frac{D^2}{2w^2}})}(e^{-\frac{X^2}{2w^2}} - \frac{1}{2}e^{-\frac{(X+D)^2}{2w^2}} - \frac{1}{2}e^{-\frac{(X-D)^2}{2w^2}})] \propto \iint dxdy \left| E_{(1,0)}(x-\frac{X}{2},y) - E_{(1,0)}(x+\frac{X}{2},y) \right|^2, \tag{10}$$

when using a QHG(1,0) beam as the spatial distribution. The power change by the displacement ΔX is expressed by

$$\frac{dI_{(1,0)}}{dX} = I_0 \frac{1}{(1-e^{-\frac{D^2}{2w^2}})}(\frac{X}{w^2}e^{-\frac{X^2}{2w^2}} - \frac{X+D}{2w^2}e^{-\frac{(X+D)^2}{2w^2}} - \frac{X-D}{2w^2}e^{-\frac{(X-D)^2}{2w^2}}). \tag{11}$$

#261242 Received 16 Mar 2016; revised 22 Apr 2016; accepted 27 Apr 2016; published 24 May 2016

The power for HG(0,0) and QHG(1,0) is compared in Fig. 6, which displays the normalized functional shapes for Eqs. (5), (7), (10), and (11), i.e., the power I and its first derivative dI/dX for the HG(0,0) and QHG(1,0) beams as a function of X at the dark port of the Sagnac interferometer.

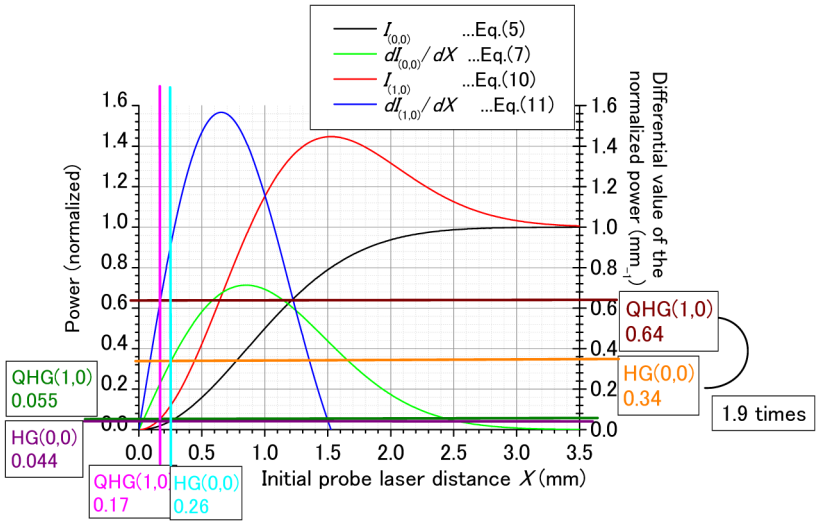

Fig. 6. The detected power I for the HG(0,0) (black line) and QHG(1,0) (red line) beams, and the differential of $I_{(0,0)}$ (green line) and $I_{(1,0)}$ (blue line) as a function of X, the lateral displacement between the CW and CCW beams at the dark port of the Sagnac interferometer. The power is normalized to the intensity when the two beams are completely separated. The powers of the interfered light of HG(0,0) and QHG(1,0) detected at the photodiode were 7.9 μA and 0.1 μA, respectively, while the powers of them with little interference measured at X = 3.4 mm were 180 μA and 1.8 μA. The powers of 7.9 μA and 0.1 μA were normalized to 0.044 (violet line) and 0.055 (dark green line), respectively, by the corresponding values with little interference. From these values and numerical calculation of the powers for HG(0,0) and QHG(1,0) by Eqs. (5) and (7), the initial probe laser distances X were estimated to be 0.26 mm (sky blue line) and 0.17 mm (pink line) respectively. The differential values of the normalized power dI/dX were also calculated to be 0.34 mm^{-1} (orange line) and 0.64 mm^{-1} (brown line). The ratio of $dI_{(1,0)}/dX$ to $dI_{(0,0)}/dX$ was 1.9, indicating the sensitivity of the displacement was improved by 1.9 times by converting HG(0,0) to QHG(1,0) when the initial probe laser distances were X = 0.26 mm for HG(0,0) and X = 0.17 mm for QHG(1,0).

The change in the light intensity by the displacement ΔX is increased for QHG(1,0) compared with that for HG(0,0). If the initial distance X is 0, then dI/dX is also 0. In order to obtain a large dI/dX value, X is set to an appropriate value.

In fact, there is an intensity difference between the two Gaussian beams reflected by a cover glass. The intensity ratio of the two Gaussian beams composing QHG(1,0) was 89%, but the calculation result of Eq. (11) changes only by 5% even if the intensity difference is considered. So the intensity difference between two Gaussian beams is not considered when the detection limit of temperature change is evaluated in section 5-1.

The improvement of the detection sensitivity is experimentally demonstrated below by this mechanism.

3. Experimental

The experimental optical setup of the QHG(1,0) beam Sagnac interferometer PDS is illustrated in Fig. 2. A 633 nm He-Ne laser (R-32734, Newport) was used as the probe laser source. The excitation light source was a white-light Xe lamp (150 W, Hamamatsu Photonics,

#261242 Received 16 Mar 2016; revised 22 Apr 2016; accepted 27 Apr 2016; published 24 May 2016

L11034) monochromated with a spectrometer, and modulated with a chopper at an appropriate modulation frequency, which was used as the reference frequency for lock-in detection performed with a lock-in amplifier (Signal Recovery 7265). The measuring time is 15 seconds for each excitation wavelength data point with 5 seconds lock-in time constant. The CW and CCW probe laser beams interfere at the dark port and are detected with a PD (Hamamatsu Photonics, S1226-8BQ). The effective area of photodiode was 5.8 mm × 5.8 mm. The output from the PD was delivered to the lock-in amplifier. The light intensity change detected with the PD, which was synchronized with the pump modulation frequency, was phase sensitively detected.

4. Results

Figure 7 shows the measurement results, where the modulation frequency was 20 Hz, the deflection medium was air, and the beam patterns of the probe laser beam were HG(0,0) and QHG(1,0) .

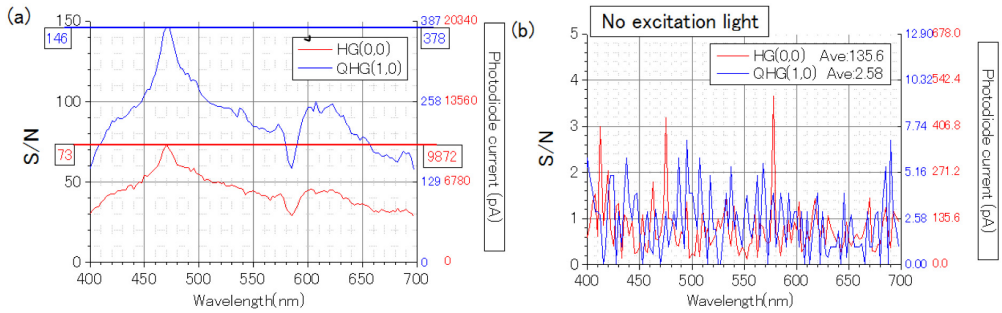

Fig. 7. PDS measurement results for a nanodiamond powder with HG(0,0) and QHG(1,0) beams (Fig. 7(a)) with a 20 Hz modulation frequency and air as the deflection medium. Each data point was measured for 15 seconds with 5 seconds lock-in time constant. The noise intensity was measured without the excitation light (Fig. 7(b)).

The samples were nanodiamond powders. The measured signal spectra were converted into the absorption spectra by normalization to the excitation light spectral shape. The probe laser beam intensity was reduced by 1/100 when the beam spatial pattern was converted from HG(0.0) to QHG(1.0). This decrease is due to the low reflectivity of the cover glass and the interference of the beams. The improvement in the S/N was demonstrated to be approximately 2.0 times. Detailed inspection in Sec. 5-1 with Fig. 6 below shows that the increase in the value of dI/dX is expected to be 1.9 times. The experimental result thus shows good agreement with the calculation.

5. Discussion

5.1. Evaluation of detection limit of temperature change

The detection limit of the temperature change, displacement, and deflection was estimated from the experimentally detected signal and the calculated interference intensity. From the measurement result shown in Fig. 7(a) and 7(b), the displacement X and the angular change $\Delta\theta$ are calculated at the detector position. The displacement X and the deflection angle $\Delta\theta$ of the probe laser beam could be estimated from the initial power, the maximum power, and the numerical calculation results from Eqs. (5), (7), (10), and (11) given in Fig. 6. The light intensity was converted to a current at the PD after the Sagnac interferometer.

The initial power was 7.9 μA based on the results in Fig. 7(a), where the maximum power that corresponds to two completely separated beams was 180 μA for HG(0,0). This was obtained by keeping the two beams apart and measuring the intensity of each beam separately. The initial power (7.9 μA) was normalized by the maximum power 180 μA to be 0.044, and is

#261242 Received 16 Mar 2016; revised 22 Apr 2016; accepted 27 Apr 2016; published 24 May 2016

shown as the violet line in Fig. 6. The initial probe laser distance X (sky blue line in Fig. 6) was then obtained as X = 0.26 mm from the intersection of the violet line and $I_{(0,0)}$ (black line in Fig. 6). The value for $dI_{(0,0)}/dX$ was determined to be 0.34 mm^{-1} from the intersection of the initial probe laser distance X and $dI_{(0,0)}/dX$ (green line in Fig. 6), which is shown as the orange line in Fig. 6. With the known values of the maximum power 180 μA detected at the photodiode, 0.34 mm^{-1} for $dI_{(0,0)}/dX$, the initial probe laser distance X = 0.26 mm, and the signal intensity 0.987 nA at the measured spectral peak wavelength, from the following equation:

$$180(\mu\text{A})\times\frac{dI_{(0,0)}}{dX}\Delta X = 0.987(\text{nA}), \tag{12}$$

the displacement ΔX is estimated to be 16 nm.

The angular change $\Delta\theta$ is then estimated from the displacement ΔX from

$$\Delta X = L_{\text{CW-CCW}}\tan\Delta\theta. \tag{13}$$

Here, $L_{\text{CW-CCW}} = L_{\text{CW}} - L_{\text{CCW}}$ is the difference in the optical light path length between the CW and CCW beams from the sample position in the Sagnac interferometer. From the displacement of ΔX = 16 nm and $L_{\text{CW-CCW}}$ = 1.10 m, $\Delta\theta$ is calculated to be 8.3 × 10^{-7}°. The corresponding temperature change is estimated with Eqs. (3) and (4). In the experiment, the excitation light irradiated region within a circle with a diameter R is 1.0 mm. The laser beam waist $2r$ at the sample position was evaluated to be 0.58 mm from the lens with the focal length of 1000 mm. The thermal diffusion length μ_{th} was calculated to be 0.59 mm. Therefore, the value for the refractive index variation $\Delta n = n_0'' - n_0'$ was calculated to be 8.4 × 10^{-9}, assuming that n_0'' is almost equal to n_0', the refractive index of air. The temperature coefficient of the refractive index dn/dT of air is 9.7 × 10^{-7} K^{-1}; therefore, the value for the temperature change ΔT just above the excitation-light irradiated spot is estimated to be 8.7 × 10^{-3} K.

The S/N of 73 and 146 are obtained at the measurement peak wavelength for the nanodiamond powders with HG(0,0) and QHG(1,0) for 15 seconds measuring time with 5 seconds lock-in time constant respectively, and the detection limits of temperature change are estimated to be 1.2 × 10^{-4} K and 5.9 × 10^{-5} K with ΔT = 8.7 × 10^{-3} K divided by the peak values for the S/N, 73 and 146, respectively. In addition, the detection limits for the angle change are estimated to be 1.1 × 10^{-8}° and 5.7 × 10^{-9}° in this spectral range with $\Delta\theta$ divided by the maximum values for the S/N. Thus, in this measurement, a twofold improvement in the S/N was successfully achieved by converting the transverse mode of the probe laser beam from the HG(0,0) beam to the QHG(1,0) beam in the spectral region from 400 to 700 nm. In this way, the detection limits for the temperature change and the deflection angle with QHG(1,0) are evaluated to be 5.9 × 10^{-5} K and 5.7 × 10^{-9}°, respectively. (In the previous paper [9], there is an error in the estimated value for the detection limit of temperature change with HG(0,0), which should be corrected from 10^{-5} K to 1.2 × 10^{-4} K.)

The intensity of the excitation light was 15 μW after the spectrometer at 650 nm. The elevated temperature T is calculated by

$$T = \frac{W_1}{\rho V C_p}, \tag{14}$$

#261242 Received 16 Mar 2016; revised 22 Apr 2016; accepted 27 Apr 2016; published 24 May 2016

where V is the volume of the hemisphere characterized by the thermal diffusion length μ_{th}, C_{p} is the specific heat of air (1006 J/kg·K), W_1 is the excitation light energy, and ρ is the density of air (1.166 kg/m^3). Thus, the excitation light intensity is converted to a temperature increase of 0.98 K at the modulation frequency of 20 Hz, if the conversion efficiency is assumed to be 100%. In fact, the value for the temperature change of air used as deflection medium is estimated to be 8.7×10^{-3} K in the experiment, indicating that almost all of the excitation light energy was used for temperature rise in the sample.

5.2. Possible origin of noise

Considering the effect of the light shot noise, the S/N is improved proportionally to the square root of the number of photons. The maximum power of the QHG(1,0) beam was approximately 1/100 compared with that of the HG(0,0) beam. This contradicts the improved S/N attained experimentally if the noise in the measurement system was dominated by shot noise, indicating that there should be major noise components other than photon shot noise. The S/N attained is in close agreement with that calculated considering only the effect of the beam pattern transformation. This observation shows that the dominant noise factor of the system is linearly correlated with the probe laser beam intensity. The photon number N was calculated by the following equation by using the value of the photodiode current 7.9 μA, the conversion efficiency 0.34 A/W of the photodiode, the photon energy of 633nm (1.958 eV) He-Ne laser, and the elementary charge 1.60×10^{-19} C as

$$N = 7.9\mu\mathrm{A} \Big/ \left(0.34\left[\mathrm{A/W}\right]\times1.958\times1.60\times10^{-19}\left[\mathrm{J}\right]\right) = 7.42\times10^{13}\left[1/\mathrm{s}\right]. \qquad (15)$$

The shot noise is given by the square root of the average photon number. The current value for the shot noise $I_{\text{shot noise}}$ is estimated as follows:

$$I_{\text{shot noise}} = 0.34\left[\mathrm{A/W}\right]\times1.958\times1.60\times10^{-19}\left[\mathrm{J}\right]\times\sqrt{N} = 0.92\mathrm{pA}/\sqrt{\mathrm{Hz}}. \qquad (16)$$

For HG(0,0), the shot noise is estimated to be $0.92\ \mathrm{pA}/\sqrt{\mathrm{Hz}}$ and the noise intensity due to the photon shot noise at 20 Hz modulation frequency is estimated to be 4.11 pA by multiplying sqrt 20 Hz ($4.47\sqrt{\mathrm{Hz}}$) with $0.92\ \mathrm{pA}/\sqrt{\mathrm{Hz}}$, while the measured average noise was 135.6 pA. The vibrational noise in the optical system was suppressed by the Sagnac interferometer because of the common optical path. Therefore, it is most likely that the main components of noise were correlated linearly with the interference light intensity of the probe laser beams. From this, the S/N improvement is explained by two factors: the twofold improvement in the sensitivity (dI / dX) as shown in Fig. 7, and the dominant noise which is linearly correlated with the probe laser beam intensity. In this experiment, the QHG(1,0) beam power was approximately 1/100 compared with that of the HG(0,0) beam. Thus, the 2 times increase in the sensitivity dI / dX and the 1/100 decrease in the probe beam power yield the $2 \times 1/100$ times signal intensity. Since the noise was also reduced to 1/100, the S/N of 2 was achieved. A further improvement in the sensitivity is thus expected by eliminating these linear noise components if, for example, subtractive detection of the probe light is incorporated in the measurement system.

5.3. Calculation for further improvement in displacement sensitivity

We used two zero order Hermite Gaussian beams and the first order quasi Hermite Gaussian beams in the present experiment. Theoretically, a more improvement in the displacement sensitivity is attainable with higher order Hermite Gaussian beams, as shown by a numerical

#261242 Received 16 Mar 2016; revised 22 Apr 2016; accepted 27 Apr 2016; published 24 May 2016

calculation below. The electric field of the Hermite Gaussian beam is represented by the following equation:

$$E_{\mathrm{HG(n,m)}}(x,y,z) \propto \exp(-ik\frac{(x^2+y^2)}{R''})\exp(-\frac{(x^2+y^2)}{w})H_{\mathrm{n}}(\frac{\sqrt{2}}{w}x)H_{\mathrm{m}}(\frac{\sqrt{2}}{w}y)\xi(z), \quad (17)$$

where H_{m} and H_{n} are the m-th and n-th order Hermite polynomials, k is the wave number of the laser beam, ξ is the Gouy phase, R'' is the radius of the curvature of the wave front. The amplitude of the electric field of the HG(n,0) beam in the xy plane is represented by

$$E_{\mathrm{HG(n,0)}}(x,y) \propto H_n(\frac{\sqrt{2}}{w}x)\exp(-\frac{(x^2+y^2)}{w}). \quad (18)$$

The power of the two n-th order Hermite Gaussian beams displaced by X is calculated as

$$I_{\mathrm{HG(n,0)}} \propto \iint dxdy\left|E_{(\mathrm{n,0})}(x-\frac{X}{2},y)-E_{(\mathrm{n,0})}(x+\frac{X}{2},y)\right|^2. \quad (19)$$

Thus, the power and the differential of the first and second order Hermite Gaussian beams are represented by

$$I_{\mathrm{HG(1,0)}} = I_0(1-(1-\frac{X^2}{w^2})e^{-\frac{X^2}{2w^2}}), \quad (20)$$

$$I_{\mathrm{HG(2,0)}} = I_0(1-(1-\frac{2X^2}{w^2}+\frac{X^4}{2w^4})e^{-\frac{X^2}{2w^2}}), \quad (21)$$

$$\frac{dI_{\mathrm{HG(1,0)}}}{dX} = I_0(\frac{3X}{w^2}-\frac{X^3}{w^4})e^{-\frac{X^2}{2w^2}}, \quad (22)$$

$$\frac{dI_{\mathrm{HG(2,0)}}}{dX} = I_0(\frac{5X}{w^2}-\frac{4X^3}{w^4}+\frac{X^5}{2w^6})e^{-\frac{X^2}{2w^2}}. \quad (23)$$

Figure 8 shows these calculation results. The ratios in the peak value of $dI_{\mathrm{HG(2,0)}}/dX$ and $dI_{\mathrm{HG(1,0)}}/dX$ to $dI_{\mathrm{HG(0,0)}}/dX$ are 3.0 and 2.3, respectively. The results demonstrate that a more improvement in the displacement sensitivity is realized with a higher order spatial beam pattern as the probe laser beam.

#261242 Received 16 Mar 2016; revised 22 Apr 2016; accepted 27 Apr 2016; published 24 May 2016

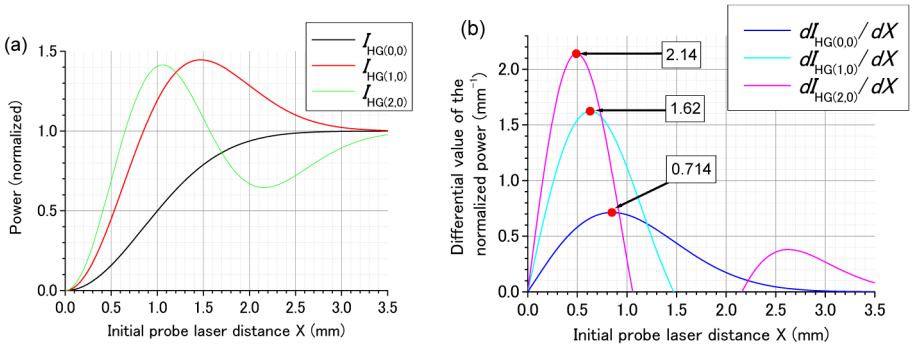

Fig. 8. The calculated power and differential of the HG(1,0), HG(2,0) modes. The radius of the beam is taken to be the same as in the experiment. The peak differential value increases with the order of the Hermite Gaussian beam.

6. Conclusion

In Sagnac interferometer PDS, we have experimentally obtained a twofold improvement in the S/N by converting the spatial beam pattern of the probe laser beam from a zero-order to a quasi first-order HG beam using air as the deflection medium and a Xe white-light lamp with a He-Ne laser as the respective excitation and probe light sources. The detection limits for temperature change with HG(0,0) and QHG(1,0) are estimated to be 1.2×10^{-4} and 5.9×10^{-5} K, respectively, in the wide spectral range from 400 to 700 nm. Accordingly, the detection limits for the deflection angle are 1.1×10^{-8}° and 5.7×10^{-9}°. It is theoretically predicted that the sensitivity is further improved for the higher order Hermite Gaussian beams. These improvements demonstrate that a higher-order HG beam Sagnac PDS is a highly sensitive, versatile method for measurement of photothermal spectra.

Acknowledgment

The authors wish to thank Ryo Kumabara and Yoshikazu Homma for providing nanodiamond powders.

#261242 Received 16 Mar 2016; revised 22 Apr 2016; accepted 27 Apr 2016; published 24 May 2016